

Energy & Environmental Science

Accepted Manuscript



This is an *Accepted Manuscript*, which has been through the Royal Society of Chemistry peer review process and has been accepted for publication.

Accepted Manuscripts are published online shortly after acceptance, before technical editing, formatting and proof reading. Using this free service, authors can make their results available to the community, in citable form, before we publish the edited article. We will replace this *Accepted Manuscript* with the edited and formatted *Advance Article* as soon as it is available.

You can find more information about *Accepted Manuscripts* in the [Information for Authors](#).

Please note that technical editing may introduce minor changes to the text and/or graphics, which may alter content. The journal's standard [Terms & Conditions](#) and the [Ethical guidelines](#) still apply. In no event shall the Royal Society of Chemistry be held responsible for any errors or omissions in this *Accepted Manuscript* or any consequences arising from the use of any information it contains.

	and Chemical Engineering; California Institute of Technology, Beckman Institute and Molecular Materials Research Center; California Institute of Technology, Kavli Nanoscience Institute

SCHOLARONE™
Manuscripts

**Interface Engineering of the Photoelectrochemical Performance of Ni-Oxide-Coated
n-Si Photoanodes by Atomic-Layer Deposition of Ultrathin Films of Cobalt Oxide**

Xinghao Zhou^{1,2†}, Rui Liu^{1†}, Ke Sun^{1,3†}, Dennis Friedrich^{1,4}, Matthew T. McDowell^{1,3}, Fan Yang^{1,3}, Stefan T. Omelchenko^{1,2}, Fadl H. Saadi^{1,2}, Adam C. Nielander³, Sisir Yalamanchili^{1,2}, Kimberly M. Papadantonakis^{1,3}, Bruce S. Brunschwig^{1,5}, Nathan S. Lewis^{1,3,5,6*}

¹Joint Center for Artificial Photosynthesis, California Institute of Technology, Pasadena, CA 91125, USA

²Division of Materials Science, California Institute of Technology, Pasadena, CA 91125, USA

³Division of Chemistry and Chemical Engineering, California Institute of Technology, Pasadena, CA 91125, USA

⁴Institute for Solar Fuels, Helmholtz-Zentrum Berlin für Materialien und Energie, Hahn-Meitner Platz 1, 14109 Berlin, Germany

⁵Beckman Institute and Molecular Materials Research Center, California Institute of Technology, Pasadena, CA 91125, USA

⁶Kavli Nanoscience Institute, California Institute of Technology, Pasadena, CA 91125, USA

† These authors contributed equally

*Corresponding author: nslewis@caltech.edu

Abstract:

Introduction of an ultrathin (2 nm) film of cobalt oxide (CoO_x) onto n-Si photoanodes prior to sputter-deposition of a thick multifunctional NiO_x coating yields stable photoelectrodes with photocurrent-onset potentials of ~ -240 mV relative to the equilibrium potential for $\text{O}_2(\text{g})$ evolution and current densities of ~ 28 mA cm^{-2} at the equilibrium potential for water oxidation when in contact with 1.0 M $\text{KOH}(\text{aq})$ under 1 sun of simulated solar illumination. The photoelectrochemical performance of these electrodes was very close to the Shockley diode limit for moderately doped n-Si(100) photoelectrodes, and was comparable to that of typical protected Si photoanodes that contained buried Si p-n junctions.

Broader context:

Thick (> 50 nm) multifunctional NiO_x coatings enable the use of small-band-gap non-oxide semiconductors as photoanodes in fully integrated, intrinsically safe, and efficient photoelectrosynthetic water-splitting systems. The equivalent open-circuit voltage generated by such protected n-type semiconductor heterojunction structures is however significantly lower than that obtained from homogeneous np^+ buried junctions. We demonstrate herein that deposition of a thin cobalt oxide film onto n-Si substrates prior to deposition of a thick multifunctional NiO_x coating significantly improves the performance of such protected n-type Si photoanodes. The approach provides a route

to formation of stabilized, high-performance Si photoanodes without requiring the formation of buried p-n homojunctions, potentially simplifying the photoelectrode processing and thus reducing the cost of monolithically integrated solar-driven water-splitting devices.

Graphical Abstract:

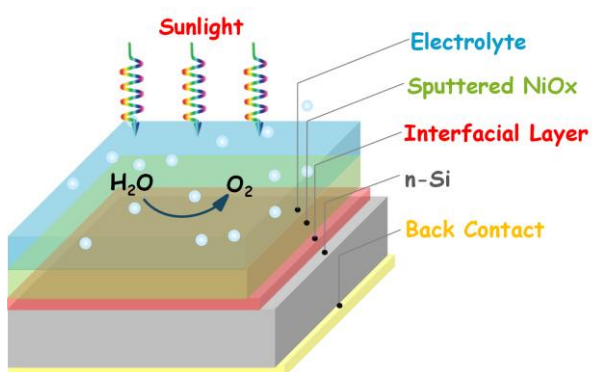


Table of contents: n-Si/SiO_x/CoO_x/NiO_x photoanodes show high water oxidation current, and 1700 h stability in 1.0 M KOH biased at 1.63 V versus RHE under 1 Sun illumination of 100 mW cm⁻².

Main text:

Although SrTiO₃, KTaO₃, and TaON have been used in stable wired or “wireless” configurations to effect direct solar-driven water splitting,¹ all known smaller-band-gap, non-oxide semiconductors require protection from corrosion for use in stable, intrinsically safe, efficient photoelectrosynthetic or photovoltaic-(PV) biased electrochemical water-splitting cells.^{2,3} When the protective layer fully prevents

contact between the electrolyte and the semiconductor, effective charge separation in the light absorber requires a mechanism for establishing a significant electric field at the semiconductor surface. Semiconductor/metal Schottky barriers;^{4,5} p-n homojunctions on planar electrodes,⁶⁻¹⁰ spherical electrodes,¹¹ and radial emitters on microwires;¹² metal-insulator-semiconductor contacts;^{13,14} in situ formation of emitter layers by carrier inversion;¹⁵⁻¹⁸ heterojunctions;¹⁹⁻²¹ and mixed barrier-height semiconductor/metal/oxide/liquid systems²² have all been investigated in either wired or “wireless” photoelectrosynthetic or PV-biased electrosynthetic systems. Generally tandem structures or triple junctions are required to provide the open-circuit voltage (V_{oc}) necessary to effect unassisted water splitting in either a wired or monolithically integrated (“wireless”) configuration,²³⁻²⁸ with noble metals or earth-abundant electrocatalysts²⁸ used in the full water-splitting system. The electrode surfaces require both protection or stabilization against corrosion and the deposition of an effective catalyst for use in either the photoelectrochemical anodic (water oxidation) or cathodic (fuel formation) half reactions.

Ni-oxide films formed by reactive sputtering have recently been shown to form protecting layers on a variety of semiconductor surfaces, including Si, InP, amorphous hydrogenated Si (a-Si:H), and CdTe.²⁹⁻³¹ The NiO_x is optically transparent in the visible region and has an index of refraction that makes the NiO_x a near-optimal anti-reflective coating on a variety of semiconductor surfaces. Furthermore, NiO_x is chemically stable at high pH, and upon activation forms a surface layer that is catalytic for the

oxygen-evolution reaction (OER), with overpotentials of ~ 330 mV at 10 mA cm^{-2} in 1.0 M KOH(aq) .²⁹ NiO_x coatings on semiconductors that form passive films under photoanodic conditions have produced high photocurrent densities for solar-driven OER from water for months of continuous operation under simulated 1 Sun conditions.²⁹⁻³¹

However, due to nonoptimal energetics at the interface between the NiO_x and the semiconductor, formation of a direct heterojunction contact between the n-type absorber and the p-type NiO_x layer yields relatively low V_{oc} values.²⁹⁻³¹ Significantly higher V_{oc} values for such stabilized systems have been obtained from electrodes formed by deposition of a NiO_x coating onto a buried p-n homojunction.^{29, 30} For example, freshly etched n-Si and np^+ -Si photoanodes protected by a multifunctional layer of NiO_x yielded equivalent open-circuit voltages (see Supplementary Information) of 180 mV and 510 mV, respectively.²⁹ The formation of heterojunctions between n-Si coated with a layer of SiO_x (either native or introduced by processing steps) and thin (< 20 nm) films of Ni,²² MnO_x ,³² and TiO_2 ³³ offers some protection against corrosion to n-Si photoanodes, and in some cases yields photoanodes exhibiting $V_{oc} \geq 500$ mV. The ideal regenerative solar-to- O_2 conversion efficiency³⁴ of these heterogeneous systems is relatively low compared to values exhibited by NiO_x protected np^+ -Si photoanodes.^{29, 35} The solar-to-fuel conversion efficiency is thus limited when such protected photoanodes are used in a tandem photochemical diode design.^{3, 36}

For technologically well-developed semiconductors such as Si and the III-V materials, p-n homojunctions can be formed to provide V_{oc} values that can approach the Shockley

diode bulk recombination/diffusion limit.^{2,3} Many semiconductors of interest for use in photoelectrochemical cells, however, cannot be doped to form high-quality homojunctions. Moreover, the doping/diffusion process generally requires high temperatures, and adds complexity to the formation of a functional photoelectrode, relative to electrodeposition or spray pyrolysis of the active semiconductor layer onto a suitable substrate. For small grain-size polycrystalline films, dopants often migrate preferentially along grain boundaries, especially during the drive-in step, producing majority-carrier shunts that degrade the performance of the resulting photoelectrode.³⁷ Hence methods which allow large V_{oc} values and high efficiencies to be obtained from protected semiconductor photoelectrodes in contact with aqueous electrolytes, but which do not require the formation of diffused homojunctions, are desirable.

We demonstrate herein that introduction of a thin, compositionally controlled, interfacial cobalt oxide layer between the n-Si absorber and the protective, multifunctional NiO_x film can yield V_{oc} values close to the Shockley diode limit for moderately doped n-Si(100) photoelectrodes. The performance and stability of such materials used as PV-biased electrosynthetic systems for water oxidation are comparable to that observed from diffused Si p-n homojunctions protected by the NiO_x overlayer. Such “interfacial engineering” of the junction energetics demonstrates that protection schemes can be implemented to yield high-performance photoelectrodes without the complexity of the requirement to form a diffused homojunction, while concurrently obtaining efficient separation of photogenerated charges in the semiconducting

photoelectrode.

To form the desired interfacial layers, n-Si (100) (0.1–1 ohm-cm resistivity, 525 μm thick) was first etched in an RCA SC-2 etchant solution for 10 min at 75 $^{\circ}\text{C}$ to produce a thin SiO_x layer on the Si surface (n-Si/ $\text{SiO}_{x,\text{RCA}}$). Thin films of CoO_x were then deposited by atomic-layer deposition (ALD) onto the Si/ $\text{SiO}_{x,\text{RCA}}$. After ALD growth of the CoO_x layer, NiO_x was deposited by reactive radio-frequency sputtering onto the CoO_x , with the Si substrates maintained at 300 $^{\circ}\text{C}$ (n-Si/ $\text{SiO}_{x,\text{RCA}}$ / CoO_x / NiO_x). Sixty ALD cycles of CoO_x deposition were found to optimize the photocurrent-onset potentials relative to the formal potential, $E^{\circ}(\text{Fe}(\text{CN})_6^{3-/4-})$ for the n-Si/ $\text{SiO}_{x,\text{RCA}}$ / CoO_x / NiO_x devices (Figure S1) and were thus used in the fabrication of all of the devices described herein.

Figure 1A shows a high-resolution transmission-electron microscopy (TEM) image of the n-Si/ $\text{SiO}_{x,\text{RCA}}$ / CoO_x / NiO_x interface. An amorphous ~ 2 nm thick layer of SiO_x was observed on the surface of the crystalline Si, with a 2–3 nm thick layer of CoO_x between the SiO_x and NiO_x layers. The low difference in contrast between the CoO_x and NiO_x layers is due to the similar densities of the metal oxide films. Figure 1B shows the results of a scanning transmission-electron microscopy (STEM) energy-dispersive spectroscopy (EDS) line scan across the n-Si/ $\text{SiO}_{x,\text{RCA}}$ / CoO_x / NiO_x interface. A Co X-ray signal was evident at the interface between the Si and Ni signals, and confirmed the presence of the thin CoO_x layer, which was also detected using X-ray photoelectron spectroscopy (XPS) (Figure S2A, B). Peak-fitting of the XP spectra in the Co $2p_{3/2}$ region

showed the co-presence of Co(II) and Co(III), possibly in the forms of CoO, Co₂O₃, Co₃O₄ and Co(OH)₂/CoOOH.^{38, 39} Grazing incidence X-ray diffractometry (GIXRD) showed that the film was polycrystalline with peak positions consistent with Co₃O₄, and indicated that annealing the film under the deposition conditions did not result in any significant changes to the structure, crystallinity, or preferred orientation of the film (Figure S2C). The root-mean-squared (rms) surface roughness of the n-Si/SiO_{x,RCA} and n-Si/SiO_{x,RCA}/CoO_x surfaces was 0.403 nm and 0.453 nm, respectively (Figure S3). A low-magnification high-angle annular dark-field (HAADF) STEM image of a cross-section of the n-Si/SiO_{x,RCA}/CoO_x/NiO_x film (Figure 1C) showed that the NiO_x film consisted of short columns with an average diameter of ~20 nm and an average height of ~102 nm, with a mean density of ~2500 columns μm⁻².

Figure 2A shows the current-density versus potential (*J-E*) behavior of n-Si/SiO_{x,RCA}/NiO_x photoanodes with and without an interfacial layer of CoO_x, in contact with 1.0 M KOH(aq), illuminated by 1 sun of simulated solar illumination, and without correction for resistance losses in the system. The photocurrent-onset potentials were -239 ± 3 mV and -74 ± 12 mV relative to the formal potential for water oxidation ($E^{\circ}(\text{O}_2/\text{H}_2\text{O}) = 1.23$ V versus a reversible hydrogen electrode, RHE, at pH = 14) for the n-Si/SiO_{x,RCA}/CoO_x/NiO_x and n-Si/SiO_{x,RCA}/NiO_x photoanodes, respectively, with three electrodes of each type measured. Thus, the presence of the interfacial CoO_x layer between the n-Si/SiO_{x,RCA} and the NiO_x resulted in a -165 mV shift in the

photocurrent-onset potential of the n-Si/SiO_{x,RCA}/CoO_x/NiO_x photoanode relative to the n-Si/SiO_{x,RCA}/NiO_x electrode that did not contain the CoO_x layer. The *J-E* behavior for the n-Si/SiO_{x,RCA}/CoO_x/NiO_x electrode exhibited a larger slope ($\sim 140.0 \text{ mA cm}^{-2} \text{ V}^{-1}$ measured between 1.00 V and 1.15 V versus RHE) than the *J-E* behavior of the n-Si/SiO_{x,RCA}/NiO_x electrode (slope $\sim 100 \text{ mA cm}^{-2} \text{ V}^{-1}$ measured between 1.25 V and 1.45 V vs RHE). The increased slope is attributable to a reduced series resistance and/or reduced surface recombination velocity, which could indicate that the CoO_x layer prevents further oxidation of the Si and/or damage to the existing SiO_{x,RCA} junction layer during sputter-deposition of the NiO_x film. The photocurrent density for the n-Si/SiO_{x,RCA}/CoO_x/NiO_x photoanode structure was $27.7 \pm 0.4 \text{ mA cm}^{-2}$ at $E^{\circ}(\text{O}_2/\text{H}_2\text{O})$, and the solar-to-O₂(g) ideal regenerative-cell conversion efficiency³⁴ (η_{IRC} , see Supplementary Information) was $2.1 \pm 0.2 \%$, while for the n-Si/SiO_{x,RCA}/NiO_x photoanode structure the photocurrent density was $6.3 \pm 1.5 \text{ mA cm}^{-2}$ at $E^{\circ}(\text{O}_2/\text{H}_2\text{O})$, and the η_{IRC} for solar-to-O₂(g) was $0.11 \pm 0.04 \%$, each with three electrodes of each type tested. A load-line analysis based on an equivalent-circuit model consisting of a photodiode connected in series with a dark electrolysis cell indicated that obtaining a shift in the *J-E* behavior equivalent to that observed for the n-Si/SiO_{x,RCA}/CoO_x/NiO_x photoanode relative to the p⁺-Si/NiO_x anode would require a $12.3 \pm 0.3 \%$ efficient photodiode with a V_{oc} of $565 \pm 3 \text{ mV}$ and a short-circuit photocurrent density (J_{sc}) of $32.5 \pm 0.3 \text{ mA cm}^{-2}$.³⁴ The performance of the n-Si/SiO_{x,RCA}/CoO_x/NiO_x photoanode was modestly better than that reported for a homogeneous buried-junction p⁺n-Si electrode

that had been freshly etched and directly sputtered with NiO_x (photocurrent-onset potential of -180 ± 20 mV relative to $E^{\circ}(\text{O}_2/\text{H}_2\text{O})$ and a photocurrent density of 29 ± 1.8 mA cm⁻² at $E^{\circ}(\text{O}_2/\text{H}_2\text{O})$), and was significantly improved relative to the performance of an HF-etched n-Si electrode that had been directly sputtered with NiO_x (photocurrent-onset potential of $+150 \pm 20$ mV relative to $E^{\circ}(\text{O}_2/\text{H}_2\text{O})$ and negligible photocurrent density at $E^{\circ}(\text{O}_2/\text{H}_2\text{O})$).²⁹

With these same n-Si substrates at a comparable light-limited current density, a high-quality semiconductor/liquid junction formed between a freshly etched n-Si photoanode¹⁷ and a non-aqueous solution containing a reversible, one-electron redox couple (e.g., CH₃OH-0.20 M 1,1'-dimethylferrocene (Me₂Fc⁰)-0.010 M Me₂Fc⁺) which forms an in-situ emitter by virtue of carrier inversion⁴⁰ yielded a photocurrent-onset potential of -640 mV relative to $E^{\circ}(\text{Me}_2\text{Fc}^{+/0})$ (Figure S4). We therefore expect that improvements upon the 0.56 V V_{oc} yielded by the n-Si/SiO_{x,RCA}/CoO_x/NiO_x structure could be obtained through decreasing the defect densities at the Si surface and by yet further increases in the band bending in the Si.

Figure 2B shows the wavelength-dependent external quantum yield (Φ_{ext}) for electrons collected from n-Si/SiO_{x,RCA}/CoO_x/NiO_x and np⁺-Si/NiO_x²⁹ photoanodes, respectively, in contact with 1.0 M KOH(aq) while under potentiostatic control at 1.93 V versus RHE. Figure 2B also displays the observed absorbance spectrum of an n-Si/SiO_{x,RCA}/CoO_x/NiO_x photoanode in air for light at normal incidence. The shape of

the Φ_{ext} versus wavelength behavior for the n-Si/SiO_{x,RCA}/CoO_x/NiO_x electrode was consistent with the absorbance spectrum of the NiO_x-coated Si substrate measured in air.²⁹ The n-Si/SiO_{x,RCA}/CoO_x/NiO_x photoanodes exhibited higher Φ_{ext} values at wavelengths < 500 nm relative to those of np⁺-Si/NiO_x photoanodes, indicating that the n-Si/SiO_{x,RCA}/CoO_x/NiO_x heterojunction had lower parasitic absorption losses in the near-surface layer. In the homojunction device, short-wavelength light is significantly absorbed by the thin, non-photoactive, highly doped emitter layer,²⁹ while in commercial high-efficiency Si photovoltaic devices, short-wavelength light is absorbed primarily by the heterogeneous passivation layers.⁴¹ For the n-Si/SiO_{x,RCA}/CoO_x/NiO_x photoanodes, Φ_{ext} was > 0.9 in the wavelength range of 550–780 nm, which compared favorably to Φ_{ext} values of ≤ 0.75 across the wavelength range of 400–1100 nm reported for n-Si/SiO_{x,RCA}/TiO₂/Ni photoanodes measured under similar conditions.⁴² The increased Φ_{ext} for the NiO_x-coated photoanodes at wavelengths > 550 nm was due to the anti-reflective behavior of the NiO_x coating. Consistently, NiO_x-coated n-Si photoanodes produced light-limited current densities under 1 Sun simulated AM1.5 illumination that were ~ 4.5 mA cm⁻² greater the light-limited current densities observed under such conditions from n-Si/SiO_{x,RCA}/TiO₂/Ni photoanodes.

Electrochemical impedance spectroscopy was used to determine the differential capacitance (C) of the n-Si/SiO_{x,RCA}/NiO_x, n-Si-E/CoO_x/NiO_x (where n-Si-E indicates n-Si which was freshly etched in buffered HF (aq) before the next processing step), and

n-Si/SiO_{x,RCA}/CoO_x/NiO_x electrodes, with Mott-Schottky plots (C^{-2} vs E) indicating flat-band potentials (V_{fb}) of -0.67 ± 0.02 V, -0.69 ± 0.03 V, and -0.83 ± 0.02 V versus (Fe(CN)₆^{3-/4-}), respectively (Figure 2C). The slopes in the linear regions of the C^{-2} vs E plots yielded a doping density of $\sim 10^{17}$ cm⁻³ for all electrodes, which implies a corresponding resistivity of ~ 0.09 ohm cm, close to the range of 0.1 – 1 ohm cm specified by the manufacturer of the Si wafer. Kelvin-probe force microscopy (KPFM, Figure 2D) showed that the work function of the CoO_x layer was 120 mV greater than that for n-Si/SiO_{x,RCA} surfaces, indicating that the energy-band structure at the n-Si/SiO_{x,RCA}/CoO_x interface was significantly different than that at the n-Si/SiO_{x,RCA} interface. The negative shift in V_{fb} for the n-Si/SiO_{x,RCA}/CoO_x/NiO_x electrode relative to the n-Si/SiO_{x,RCA}/NiO_x electrode is in accord with the KPFM data, as well as with the J - E behavior observed in 1.0 M KOH(aq) (Figure 2A). The barrier height within the Si of n-Si/SiO_{x,RCA}/CoO_x/NiO_x as calculated from the $0.83 \text{ V} \pm 0.02 \text{ V}$ flat-band potential was $0.98 \text{ V} \pm 0.02 \text{ V}$ (see Supplementary Information), close to the band gap of Si. This large band bending would likely result in the formation of a strong inversion layer at the surface of n-Si,⁴³ and thus would result in large observed photovoltages due to the associated improvements in charge-carrier separation and collection, as well as due to a reduction in the rate of electron-hole recombination and improvement in diffusion of charge carriers.⁴⁴

The reverse-saturation current density and the diode quality factor for the n-Si/SiO_{x,RCA}/CoO_x/NiO_x photoanode, extracted by a linear fit of the dependence of the photocurrent-onset potentials relative to $E^{\circ}(\text{Fe}(\text{CN})_6^{3-/4-})$ on the logarithm of photocurrent density (J_{ph}) (Figure S5), were $1.50 \times 10^{-7} \text{ mA cm}^{-2}$ and 1.09, respectively. The diffusion current was $\sim 10^{-10} \text{ mA cm}^{-2}$, thus the thermionic emission current was the dominant contributor to the reverse-saturation current. Given a Richardson constant of $120 \text{ A cm}^{-2} \text{ K}^{-2}$ and a barrier height of $0.98 \pm 0.02 \text{ V}$ (see Supplementary Information), the transmission coefficient, α , was estimated to be on the order of unity.

Figure 3A shows the chronopotentiometric data for an n-Si/SiO_{x,RCA}/CoO_x/NiO_x photoanode in contact with 1.0 M KOH(aq) and held at 1.63 V versus RHE while under simulated 1 sun illumination of 100 mW cm^{-2} . The current density was $30 \pm 2 \text{ mA cm}^{-2}$ for 1700 h of continuous operation, at which point the experiment was stopped. Cyclic voltammograms were collected every 10 h during the stability test (Figure 3B), and showed that the J - E behavior for the photoanode gradually shifted anodically throughout the experiment. The photocurrent-onset potential relative to $E^{\circ}(\text{O}_2/\text{H}_2\text{O})$ shifted from -239 mV to -214 mV, -198 mV, and -185 mV while the photocurrent density at $E^{\circ}(\text{O}_2/\text{H}_2\text{O})$ decreased from 27.9 mA cm^{-2} to 24.6 mA cm^{-2} , 21.4 mA cm^{-2} and 16.2 mA cm^{-2} after 500 h, 1000 h and 1500 h respectively. Hence the solar-to-O₂(g) value for η_{IRC}^{34} decreased from 2.2% to 1.5%, 1.1%, and 0.74% after 500 h, 1000 h and 1500 h of operation, respectively. The gradual decrease in performance may result from the

generation of SiO_x islands at pinholes in the sputtered NiO_x film and/or from an increase in resistivity arising from thickening of the SiO_x layer in the interface, as well as from the slow electrochemical conversion of CoO_x to $\text{Co}(\text{OH})_2$ and then to ion-permeable CoOOH (Figure S6) and the loss of catalytic activity. The stability of $\text{n-Si/SiO}_{x,\text{RCA}}/\text{CoO}_x/\text{NiO}_x$ photoanodes was comparable to the reported stability of $\text{np}^+\text{-Si/NiO}_x$ photoanodes,²⁹ demonstrating that the interfacial CoO_x layer did not adversely affect the stability of the NiO_x coating.

Figure 3C shows the mass of $\text{O}_2(\text{g})$ generated, as determined using a calibrated oxygen probe, by an $\text{n-Si/SiO}_{x,\text{RCA}}/\text{CoO}_x/\text{NiO}_x$ photoanode in contact with 1.0 M $\text{KOH}(\text{aq})$ under galvanostatic control for 30 min at a current density of 0.5 mA cm^{-2} . The measured mass of $\text{O}_2(\text{g})$ was in agreement with that calculated based on the charge passed, assuming 100% Faradaic efficiency for the generation of $\text{O}_2(\text{g})$. The total charge passed during the stability test was 1×10^7 greater than the total charge needed to dissolve the CoO_x interfacial layer, and was 1×10^2 greater than the charge required to dissolve the entire Si substrate (see Supplementary Information). Assuming a 20% solar capacity factor, the 1700 h of stable water oxidation measured for the $\text{n-Si/SiO}_{x,\text{RCA}}/\text{CoO}_x/\text{NiO}_x$ photoanode in contact with 1.0 M $\text{KOH}(\text{aq})$ represented the same amount of anodic charge density as would be passed in approximately one year of operation in the field at a maximum photocurrent density of 30 mA cm^{-2} .

The thin layer of chemically grown silicon oxide present on the n-Si substrates prior to further processing by ALD and sputtering contributes to the improvement in performance observed when comparing n-Si/SiO_{x,RCA}/CoO_x/NiO_x photoanodes to n-Si/CoO_x/NiO_x photoanodes (Figure 2C, S7). Both ALD and sputtering result in the growth of a thin layer of SiO_x on freshly etched silicon surfaces. The properties of the SiO_x layers produced by the different processing methods vary, and affect the performance of devices. The chemically grown SiO_x layer may result in fewer trap states at the Si/SiO_x interface than are produced by the sputtered SiO_x, and/or may serve to protect the underlying silicon from arcs and surface roughening during the RF sputtering process. In addition, the SiO_x layer likely contributes to the initiation and conformity of the ALD growth process for the CoO_x interfacial films, which on freshly etched Si surfaces would be expected to proceed via inhomogeneous island growth that can result in rough films as well as in interfacial silicon oxides or silicates,⁴⁵ and in reduced values for the built-in voltage and photovoltage of the junction.

Although this work has focused on the use of interfacial layers of ALD-grown CoO_x, other transition-metal oxides, including FeO_x and NiO_x, also hold promise for use as interfacial layers on Si photoanodes protected by sputtered NiO_x (Figure S7).

This work clearly demonstrates that the introduction of ALD layers of cobalt oxide improves the equivalent open-circuit voltage of protected n-Si photoanodes to values comparable to that obtainable from photoanodes fabricated using homogeneous p-n

buried Si junctions. Interfacial cobalt oxide layers increase the band bending at the interface and thereby offer a route to high-performance photoanodes, potentially simplifying the photoelectrode processing and allowing for the use of inexpensive polycrystalline absorbers while maintaining high photoelectrode performance.

Acknowledgement:

This work was supported by the Joint Center for Artificial Photosynthesis, a DOE Energy Innovation Hub, supported through the Office of Science of the U.S. Department of Energy under Award Number DE-SC0004993. UV-VIS spectroscopy, atomic-force microscopy, and Kelvin probe force microscopy were performed at the Molecular Materials Resource Center (MMRC) of the Beckman Institute at the California Institute of Technology. ACN was supported by a Graduate Research Fellowship from the National Science Foundation. This work was additionally supported by the Gordon and Betty Moore Foundation under Award No. GBMF1225.

Author contribution:

X.Z., R.L., K.S., K.M.P, B.S.B and N.S.L designed the experiments and wrote the manuscript. X.Z., R.L. K.S., D.F., M.T.M, Y.F., S.T.O. A.C.N., S.Y. performed the experiments.

Figures:

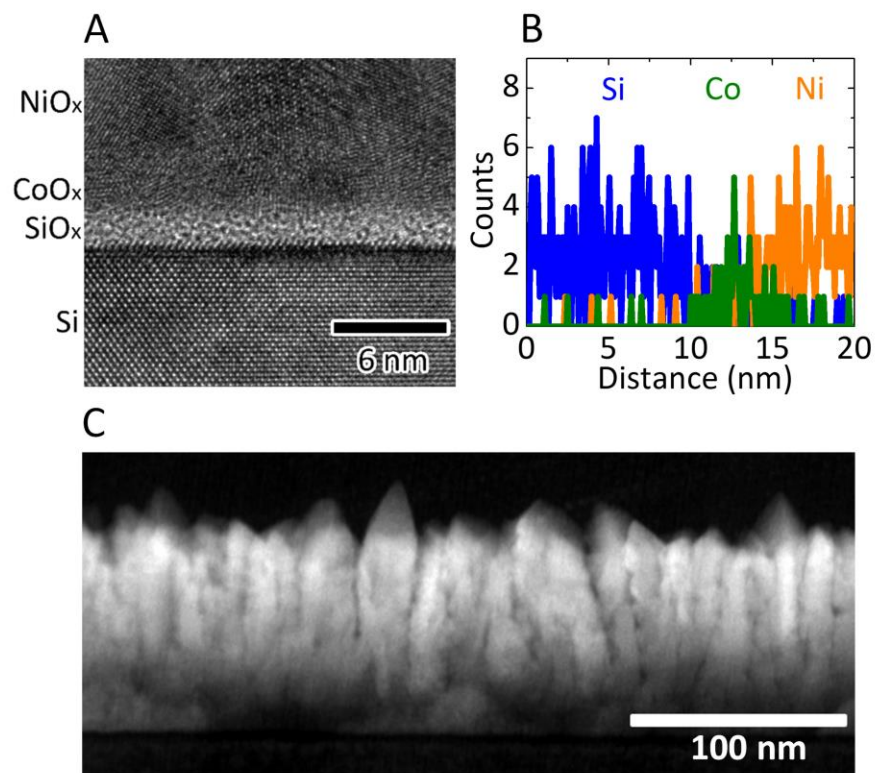


Figure 1. (A) High-resolution transmission-electron microscope (TEM) image of a cross-section of an n-Si/SiO_{x,RCA}/CoO_x/NiO_x sample. The lighter region at the surface of the Si is SiO_x. The CoO_x layer is incorporated into the highly polycrystalline region between the SiO_x and the larger NiO_x grains at the top of the image. (B) Energy-dispersive spectroscopy (EDS) line-scan across the Si/SiO_{x,RCA}/CoO_x/NiO_x interface in which the $K\alpha$ X-rays from Si, Co, and Ni are displayed as a function of distance. (C) Low-magnification HAADF-STEM cross-sectional image of an n-Si/SiO_{x,RCA}/CoO_x/NiO_x electrode. The bright film is the polycrystalline NiO_x layer, which grew in a columnar

fashion with vertical grain boundaries. The Si wafer is the dark layer at the bottom of the image.

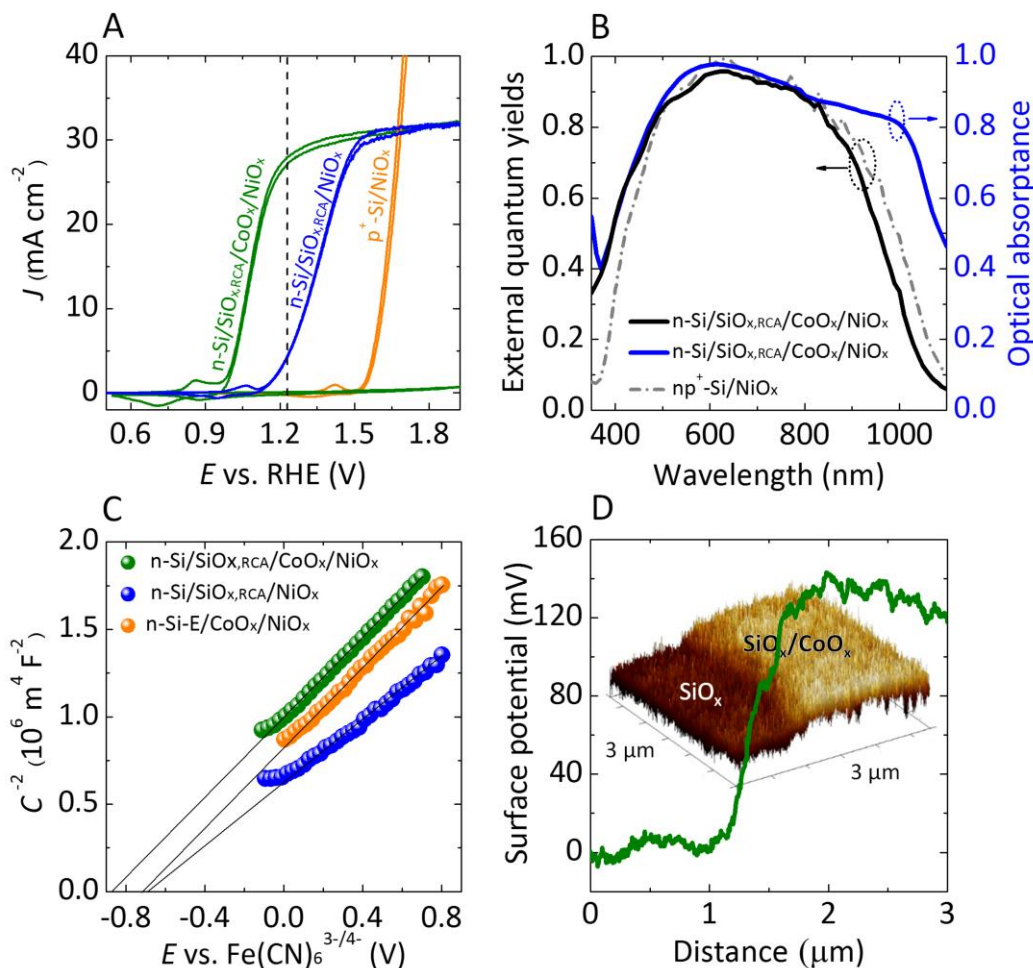


Figure 2. (A) Representative current-density versus potential (J - E) behavior of $n\text{-Si/SiO}_{x,\text{RCA}}/\text{CoO}_x/\text{NiO}_x$ and $n\text{-Si/SiO}_{x,\text{RCA}}/\text{NiO}_x$ photoanodes in contact with 1.0 M KOH (aq) in the dark (See Supplementary Information) and under 100 mW cm^{-2} of simulated AM1.5G solar illumination. The J - E behavior of a non-photoactive $p^+\text{-Si/NiO}_x$ electrode is also shown. The dark dashed line indicates the formal potential for water oxidation, $E^\circ(\text{O}_2/\text{H}_2\text{O})$. (B) Wavelength-dependent external quantum yield for

n-Si/SiO_{x,RCA}/CoO_x/NiO_x (black) and np⁺-Si/NiO_x (gray dash and dot) photoanodes in contact with 1.0 M KOH(aq) and held potentiostatically at 1.93 V versus a reversible hydrogen electrode (RHE) while illuminated by light that had been passed through a monochromator. The data for the np⁺-Si/NiO_x photoanode are extracted from reference 29. The optical absorbance for the n-Si/SiO_{x,RCA}/CoO_x/NiO_x photoanode is shown in blue. (C) Mott-Schottky (C^{-2} vs E) plots of the inverse of the differential capacitance of the electrode vs potential for an n-Si/SiO_{x,RCA}/NiO_x photoanode (blue), an n-Si-E/CoO_x/NiO_x photoanode (orange, n-Si-E indicates the n-Si was freshly etched in buffered HF (aq) before the next processing step), and an n-Si/SiO_{x,RCA}/CoO_x/NiO_x photoanode (green). (D) Kelvin probe force microscopy images showing the change in potential as the probe was scanned from the n-Si/SiO_{x,RCA} surface to the n-Si/SiO_{x,RCA}/CoO_x surface.

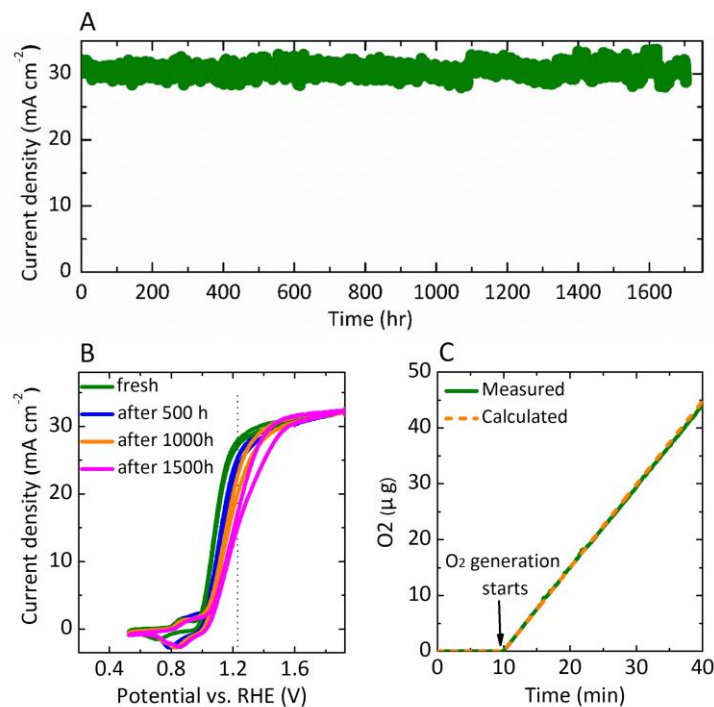


Figure 3 (A) Chronoamperometry of n-Si/SiO_{x,RCA}/CoO_x/NiO_x photoanodes biased at 1.63 V vs. RHE under 1 Sun of simulated 1.5G solar illumination from an ENH-type tungsten-halogen lamp. (B) Representative *J-E* behavior for an n-Si/SiO_{x,RCA}/CoO_x/NiO_x photoanode in contact with 1.0 M KOH(aq) under 100 mW cm⁻² of AM 1.5G simulated solar illumination collected before, and after 500 h, 1000 h and 1500 h of continuous operation at 1.63 V vs RHE. (C) Mass of O₂ (g) generated (green line) by an n-Si/SiO_{x,RCA}/CoO_x/NiO_x photoanode held at a constant current density of 0.5 mA cm⁻² for 30 min while under AM 1.5G simulated illumination and in contact with 1.0 M KOH(aq), as determined by a calibrated O₂ probe and as calculated based on the charge passed assuming 100% Faradaic efficiency for O₂ generation (orange dashed line).

References:

1. M. S. Wrighton, P. T. Wolczanski and A. B. Ellis, *J. Solid State Chem.*, 1977, **22**, 17-29.
2. M. X. Tan, P. E. Laibinis, S. T. Nguyen, J. M. Kesselman, C. E. Stanton and N. S. Lewis, *Prog. Inorg. Chem.*, 1994, **41**, 21-144.
3. M. G. Walter, E. L. Warren, J. R. McKone, S. W. Boettcher, Q. Mi, E. A. Santori and N. S. Lewis, *Chem. Rev.*, 2010, **110**, 6446-6473.
4. K. Rajeshwar, N. R. de Tacconi and C. R. Chenthamarakshan, *Chem. Mater.*, 2001, **13**, 2765-2782.
5. F. R. F. Fan, G. A. Hope and A. J. Bard, *J. Electrochem. Soc.*, 1982, **129**, 1647-1649.
6. Y. Nakato, Y. Egi, M. Hiramoto and H. Tsubomura, *J. Phys. Chem.*, 1984, **88**, 4218-4222.
7. Y. Nakato, M. Yoshimura, M. Hiramoto, A. Tsumura, T. Murahashi and H. Tsubomura, *Bull. Chem. Soc. Jpn.*, 1984, **57**, 355-360.
8. S. W. Boettcher, E. L. Warren, M. C. Putnam, E. A. Santori, D. Turner-Evans, M. D. Kelzenberg, M. G. Walter, J. R. McKone, B. S. Brunschwig, H. A. Atwater and N. S. Lewis, *J. Am. Chem. Soc.*, 2011, **133**, 1216-1219.
9. H. Morisaki, T. Watanabe, M. Iwase and K. Yazawa, *Appl. Phys. Lett.*, 1976, **29**, 338-340.
10. M. Matsumura, Y. Sakai, S. Sugahara, Y. Nakato and H. Tsubomura, *Sol. Energy Mater.*, 1986, **13**, 57-64.
11. J. D. Luttmmer, D. Konrad and I. Trachtenberg, *J. Electrochem. Soc.*, 1985, **132**, 1054-1058.
12. E. L. Warren, J. R. McKone, H. A. Atwater, H. B. Gray and N. S. Lewis, *Energy Environ. Sci.*, 2012, **5**, 9653-9661.
13. G. Hodes, L. Thompson, J. Dubow and K. Rajeshwar, *J. Am. Chem. Soc.*, 1983, **105**, 324-330.
14. J. A. Switzer, *J. Electrochem. Soc.*, 1986, **133**, 722-728.
15. W. Kautek and H. Gerischer, *Electrochim. Acta*, 1981, **26**, 1771-1778.
16. A. Heller, *Acc. Chem. Res.*, 1981, **14**, 154-162.
17. F. Gstrein, D. J. Michalak, W. J. Royea and N. S. Lewis, *J. Phys. Chem. B*, 2002, **106**, 2950-2961.
18. D. V. Esposito, I. Levin, T. P. Moffat and A. A. Talin, *Nat. Mater.*, 2013, **12**, 562-568.
19. W. Siripala, A. Ivanovskaya, T. F. Jaramillo, S. H. Baeck and E. W. McFarland, *Sol. Energy Mater. Sol. Cells*, 2003, **77**, 229-237.
20. M. Moriya, T. Minegishi, H. Kumagai, M. Katayama, J. Kubota and K. Domen, *J. Am. Chem. Soc.*, 2013, **135**, 3733-3735.
21. Y. J. Hwang, A. Boukai and P. D. Yang, *Nano Lett.*, 2009, **9**, 410-415.
22. M. J. Kenney, M. Gong, Y. G. Li, J. Z. Wu, J. Feng, M. Lanza and H. J. Dai, *Science*, 2013, **342**, 836-840.

23. O. Khaselev and J. A. Turner, *Science*, 1998, **280**, 425-427.
24. R. E. Rocheleau, E. L. Miller and A. Misra, *Energy Fuels*, 1998, **12**, 3-10.
25. S. Licht, B. Wang, S. Mukerji, T. Soga, M. Umeno and H. Tributsch, *J. Phys. Chem. B*, 2000, **104**, 8920-8924.
26. E. L. Miller, R. E. Rocheleau and X. M. Deng, *Int. J. Hydrogen Energy*, 2003, **28**, 615-623.
27. S. Y. Reece, J. A. Hamel, K. Sung, T. D. Jarvi, A. J. Esswein, J. J. H. Pijpers and D. G. Nocera, *Science*, 2011, **334**, 645-648.
28. Y. Yamada, N. Matsuki, T. Ohmori, H. Mametsuka, M. Kondo, A. Matsuda and E. Suzuki, *Int. J. Hydrogen Energy*, 2003, **28**, 1167-1169.
29. K. Sun, M. T. McDowell, A. C. Nielander, S. Hu, M. R. Shaner, F. Yang, B. S. Brunshwig and N. S. Lewis, *J. Phys. Chem. Lett.*, 2015, **6**, 592-598.
30. K. Sun, Y. Kuang, E. A. Verlage, B. S. Brunshwig, C. W. Tu and N. S. Lewis, *Adv. Energy Mater.*, 2015, DOI: 10.1002/aenm.201402276.
31. K. Sun, F. H. Saadi, M. Lichterman, W. G. Hale, H.-P. Wang, X. Zhou, N. T. Plymale, S. Omelchenko, J.-H. He, K. M. Papadantonakis, B. S. Brunshwig and N. S. Lewis, *Proc. Natl. Acad. Sci. U.S.A.*, 2015, **112**, 3612-3617.
32. N. C. Strandwitz, D. J. Comstock, R. L. Grimm, A. C. Nichols-Nielander, J. Elam and N. S. Lewis, *J. Phys. Chem. C*, 2013, **117**, 4931-4936.
33. Y. W. Chen, J. D. Prange, S. Dühnen, Y. Park, M. Gunji, C. E. D. Chidsey and P. C. McIntyre, *Nat. Mater.*, 2011, **10**, 539-544.
34. R. H. Coridan, A. C. Nielander, S. A. Francis, M. T. McDowell, V. Dix, S. M. Chatman and N. Lewis, *Energy Environ. Sci.*, 2015, DOI: 10.1039/C5EE00777A.
35. K. Sun, S. Shen, Y. Liang, P. E. Burrows, S. S. Mao and D. Wang, *Chem. Rev.*, 2014, **114**, 8662-8719.
36. A. J. Nozik, *Appl. Phys. Lett.*, 1977, **30**, 567-569.
37. A. Heller, in *Photoeffects at Semiconductor-Electrolyte Interfaces*, American Chemical Society, Washington, D.C., 1981, vol. 146, ch. 4, pp. 57-77.
38. M. C. Biesinger, B. P. Payne, A. P. Grosvenor, L. W. M. Lau, A. R. Gerson and R. S. C. Smart, *Appl. Surf. Sci.*, 2011, **257**, 2717-2730.
39. J. Yang, H. Liu, W. N. Martens and R. L. Frost, *J. Phys. Chem. C*, 2010, **114**, 111-119.
40. M. L. Rosenbluth, C. M. Lieber and N. S. Lewis, *Appl. Phys. Lett.*, 1984, **45**, 423-425.
41. H.-P. Wang, K. Sun, S. Y. Noh, A. Kargar, M.-L. Tsai, M.-Y. Huang, D. Wang and J.-H. He, *Nano Lett.*, 2015, DOI: 10.1021/nl5041463.
42. S. Hu, M. R. Shaner, J. A. Beardslee, M. Lichterman, B. S. Brunshwig and N. S. Lewis, *Science*, 2014, **344**, 1005-1009.
43. R. Memming, *Semiconductor Electrochemistry*, Wiley, Weinheim, Federal Republic of Germany, 2001.
44. Z. Zhang and J. T. Yates, *Chem. Rev.*, 2012, **112**, 5520-5551.

45. M. M. Frank, Y. J. Chabal, M. L. Green, A. Delabie, B. Brijs, G. D. Wilk, M. Y. Ho, E. B. O. da Rosa, I. J. R. Baumvol and F. C. Stedile, *Appl. Phys. Lett.*, 2003, **83**, 740-742.